JOURNAL OF APPLIED PHYSICS **113**, 143703 (2013)

Monolayer semiconducting transition metal dichalcogenide alloys: Stability and band bowing

Jun Kang,[1,2] Sefaattin Tongay,[1,3] Jingbo Li,[1,a)] and Junqiao Wu[1,2,3,b)]
[1]*State Key Laboratory of Superlattices and Microstructures, Institute of Semiconductors, Chinese Academy of Sciences, P.O. Box 912, Beijing 100083, China*
[2]*Materials Sciences Division, Lawrence Berkeley National Laboratory, Berkeley, California 94720, USA*
[3]*Department of Materials Science and Engineering, University of California, Berkeley, California 94720, USA*

(Received 20 February 2013; accepted 18 March 2013; published online 8 April 2013)

The stability and band bowing effects of two-dimensional transition metal dichalcogenide alloys $MX_{2(1-x)}X'_{2x}$ (M = Mo, W, and X, X′ = S, Se, Te) are investigated by employing the cluster expansion method and the special quasi-random structure approach. It is shown that for (S, Se) alloys, there exist stable ordered alloy structures with concentration x equal to 1/3, 1/2, and 2/3, which can be explained by the small lattice mismatch between the constituents and a large additional charge exchange, while no ordered configuration exists for (Se, Te) and (S, Te) alloys at 0 K. The calculated phase diagrams indicate that complete miscibility in the alloys can be achieved at moderate temperatures. The bowing in lattice constant for the alloys is quite small, while the bowing in band gap, and more so in band edge positions, is much more significant. By decomposing the formation of alloy into multiple steps, it is found that the band bowing is the joint effect of volume deformation, chemical difference, and a low-dimensionality enhanced structure relaxation. The direct band gaps in these alloys continuously tunable from 1.8 eV to 1.0 eV, along with the moderate miscibility temperatures, make them good candidates for two-dimensional optoelectronics. © *2013 American Institute of Physics*. [http://dx.doi.org/10.1063/1.4799126]

I. INTRODUCTION

Recently, two-dimensional (2D) transition metal dichalcogenides (TMDs) have become a focus of research efforts.[1–5] In contrast to semi-metallic graphene,[6] monolayers of many TMDs possess direct gaps, with both the valence band maximum (VBM) and conduction band minimum (CBM) located at the K (K′) point of the hexagonal Brillouin zone.[4,5,7,8] Various studies on light emission,[9] strain response,[10,11] excitonic effects,[12] valley polarization,[13,14] photoresponsivity,[15] and field-effect response[16,17] of the monolayer TMDs have demonstrated their potential in technological applications.

However, a specific monolayer TMD with chemical formula of MX_2 (M = Mo, W and X = S, Se, and Te) provides a single direct band-gap value. To integrate 2D-TMDs for advanced applications, it is desirable to extend and tune their physical properties especially the band gaps. Historically, semiconductor science and technologies have been greatly advanced by alloying different semiconductors to achieve continuously tunable electronic structures, such as Si_xGe_{1-x} for high-mobility transistors, $Al_xGa_{1-x}As$ for quantum structures, $CuIn_xGa_{1-x}Se_2$ for solar cells, $In_xGa_{1-x}N$ for light emitting diodes, and $Hg_xCd_{1-x}Te$ for infrared detectors. In this sense, alloying is a promising approach allowing one to tune the band gap (and hence the electrical and optical properties) of semiconductors. The structural, electronic, and optical properties of alloys can be tuned continuously by varying the concentration of the constituents,[18,19] thus the range of available material properties is much extended.

While alloying in conventional semiconductors is well established, the response of 2D semiconductors to alloying might be quite different due to the low dimensionality and distinct boundary conditions. For example, many 3D semiconductor alloys exhibit spontaneous long-range ordering,[20–22] but it is unknown whether the 2D semiconductors also display ordered ground state (GS) configuration. Second, it is intriguing to see how the miscibility in these 2D alloys varies as temperature changes, and at what temperature a complete miscibility can be achieved. Finally, physical properties of alloyed semiconductor often deviate from concentration-averaged values of the constituents, known as the bowing effect. Fundamentally important for material design of 2D semiconductors, these bowing effects in lattice constant, band gap, and band edge position have yet to be thoroughly analyzed.

Successful alloying of 2D TMDs has not been experimentally reported, while band structures of several molybdenum (Mo)-based dichalcogenide alloys have been calculated by Komsa and Krasheninnikov.[23] They show that these alloys can be thermodynamically stable, and the band gap can be continuously tuned while retaining the direct gap character. However, important alloy behavior such as phase diagram and atomic ordering has not been investigated; it is also not clear what electronic process is responsible for the band bowing, and whether the effects in Mo-based alloys can be extended to other TMDs in general. In this work, the stability and bowing effect of semiconducting TMD monolayer alloys $MX_{2(1-x)}X'_{2x}$ (M = Mo, W, and X, X′ = S, Se, Te) are systematically investigated in detail. Cluster expansions (CEs) of $MX_{2(1-x)}X'_{2x}$ are constructed, and are used to search for ordered configuration and to calculate the phase

a)Email: jbli@semi.ac.cn.
b)Email: wuj@berkeley.edu.

diagram at variable temperatures. We show that in (S, Se) alloys, there are stable ordered alloy structures with concentration x of 1/3, 1/2, and 2/3; however, ordered configuration is absent for (Se,Te) and (S,Te) alloys at 0 K. The special quasi-random structure (SQS) approach is employed to investigate the bowing effects in $MX_{2(1-x)}X'_{2x}$ alloys. The bowing in the alloys is found to be the joint effect of volume deformation (VD), chemical difference, and structure relaxation. The band gaps in these alloys remain direct and tunable, making them good candidates for 2D optoelectronics.

II. METHODS

The stability of $MX_{2(1-x)}X'_{2x}$ alloys at 0 K can be evaluated from their formation enthalpies ΔH, which are calculated by

$$\Delta H = E_T(MX_{2(1-x)}X'_{2x}) - xE_T(MX'_2) - (1-x)E_T(MX_2),$$

where $E_T(MX_2)$, $E_T(MX'_2)$, and $E_T(MX_{2(1-x)}X'_{2x})$ are the total energy of pure MX_2, pure MX'_2, and the mixed alloy, respectively. The value of ΔH depends on the specific atomic arrangement in the $MX_{2(1-x)}X'_{2x}$ alloys. According to the CE formalism,[24,25] the atomic arrangement can be described by assigning occupation variables σ_i to each anion site i, with σ_i equals -1 or $+1$ if the site is occupied by X or X′, respectively. Any alloy configuration can be represented by a vector $\vec{\sigma} = (\sigma_1, \sigma_2, \sigma_3, \ldots)$ containing all the σ_i information on the anion lattice. The formation enthalpy of a $MX_{2(1-x)}X'_{2x}$ configuration $\vec{\sigma}$ can be then decomposed into energy contributions of cluster figures (such as pairs, triplets, and quadruplets)

$$\Delta H(\vec{\sigma}) = \sum_{\alpha} m_\alpha J_\alpha \xi_\alpha(\vec{\sigma}),$$

where α is a cluster, and the summation is taken over all symmetry-nonequivalent clusters. m_α is the multiplicity which denotes the number of symmetry-equivalent clusters of α, and J_α is the effective cluster interaction (ECI) coefficient. ξ_α is the so-called cluster correlation function[26] for α, which is defined as

$$\xi_\alpha(\vec{\sigma}) = \left\langle \prod_{i \in \alpha'} \sigma_i \right\rangle.$$

The bracket represents the average over all symmetry-equivalent clusters α' of α. For a random alloy, the correlation function is $(2x-1)^k$, with x the concentration and k the number of sites included in the cluster. For each alloy, the formation enthalpies of more than 50 selected alloy configurations up to 24 atoms per cell were evaluated from first-principles calculations, and the cluster expansion was constructed based on the calculated values using the ATAT code.[27] 26 clusters up to quadruplet were included for the fitting of ECIs. The fitted ECIs were then used to predict the formation enthalpies of all symmetry-inequivalent alloy configurations (~17 000) up to 24 atoms per cell.

To investigate the bowing effect in $MX_{2(1-x)}X'_{2x}$ random alloy, a 6×6 hexagonal supercell containing 108 atoms was used in the calculation of electronic properties, while the distribution of the X and X′ atoms in the lattice was modeled via the SQS approach.[26,28] The most relevant correlation functions of the constructed SQS are close to those of a random alloy, so the physical properties of the random alloy can be well simulated by the SQS.

First principles calculations were performed using the Vienna *ab initio* simulation package (VASP).[29,30] The frozen-core projector augmented wave (PAW) method[31,32] and generalized gradient approximation of Perdew-Burke-Ernzerhof (GGA-PBE)[33] were employed. Energy cutoff for plane-wave expansion was set to 400 eV. Brillouin zone sampling was performed with Monkhorst-Pack (MP) special k-point meshes[34] including Γ point. For the hexagonal primitive cell, a grid of $24 \times 24 \times 1$ was used, and the k-point grid scaled with respect to the supercell size. A vacuum layer thicker than 10 Å was added to avoid interaction between adjacent images. Structural relaxation (SR) was stopped when the calculated Hellmann-Feynman force on each atom was smaller than 0.01 eV/Å. The spin-orbit interaction was not included in band structure calculations of the alloys since the difference of the spin-orbit splitting of VBM in common-cation MX_2 is small, and the corresponding contributions can be largely cancelled out when comparing the trend of the band properties. The vacuum level was taken as zero reference for the alignment of the band edge positions.

III. RESULTS AND DISCUSSIONS

A. Stability and phase diagram

The CE of all six types of $MX_{2(1-x)}X'_{2x}$ alloys were constructed, and we calculated the formation enthalpies of the alloys based on the CE. Interestingly, the (S, Se) alloys show a behavior different from the others. The formation enthalpy ΔH of (S, Se) alloys is given in Fig. 1. It is seen that for many configurations of these two alloys, ΔH is negative, implying that an ordered alloy can form spontaneously. The solid lines in Fig. 1 represent the GS configuration. When the calculated ΔH for a particular alloying configuration is on the GS line, that particular configuration is stable even at 0 K. For both $MoS_{2(1-x)}Se_{2x}$ and $WS_{2(1-x)}Se_{2x}$, there are three stable ground states, with concentration x equal to 1/3, 1/2, and 2/3. The structures of the ground states for $MoS_{2(1-x)}Se_{2x}$ are the same as $WS_{2(1-x)}Se_{2x}$, and those of $MoS_{2(1-x)}Se_{2x}$ are shown in Fig. 1. In these ground states, clustering of S or Se atoms is not energetically favored, and the S (Se) atoms prefer to occupy the neighbor sites of Se (S) atoms. For instance, in MoSSe, the mirror site of an S (Se) atom with respect to the Mo plane is occupied by a Se (S) atom. The trend of forming dissimilar atom pairs can be explained by the dominance of positive values in the ECIs of short-range pairs. In Fig. 2, the pair interaction J_{pair} for $MoS_{2(1-x)}Se_{2x}$ is plotted. That for $WS_{2(1-x)}Se_{2x}$ is quite similar. It can be seen that J_{pair} for the nearest and next nearest pairs are both positive, and the magnitude is much higher than the negative ones. Positive pair interaction leads to

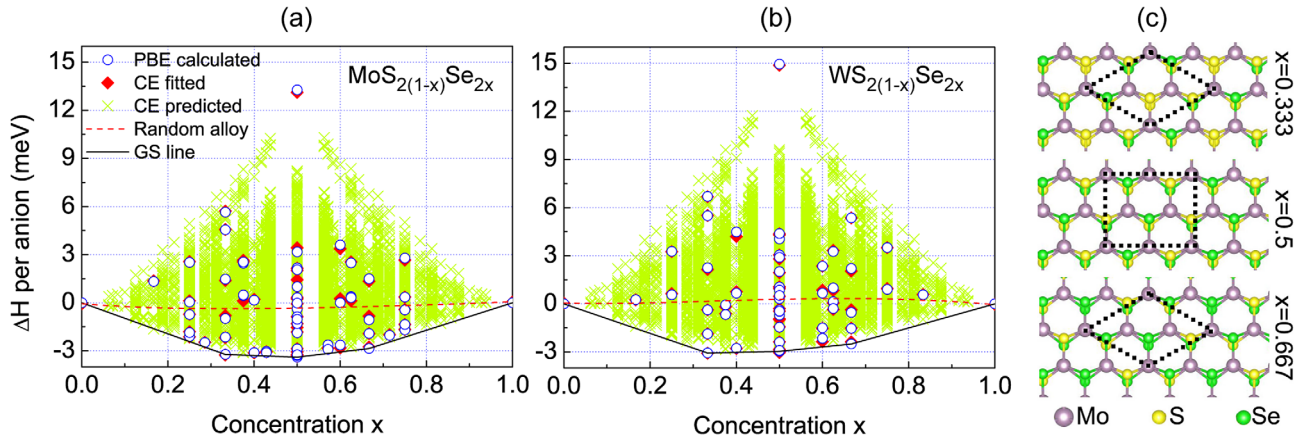

FIG. 1. (a) and (b) First-principles calculated formation enthalpies for $MoS_{2(1-x)}Se_{2x}$ and $WS_{2(1-x)}Se_{2x}$, respectively, along with the CE fitted results. The formation enthalpies predicted by CE for all symmetry-inequivalent alloy configurations (~17 000) up to 24 atoms per cell are also given. (c) The structure of ground states of $MoS_{2(1-x)}Se_{2x}$ at 0 K. The dashed lines indicate the corresponding supercells.

repulsion between anions with the same species, thus clustering is prevented.

Among the ground states of $MoS_{2(1-x)}Se_{2x}$, MoSSe has the lowest ΔH, and the stability follows MoSSe > $MoS_{4/3}Se_{2/3}$ > $MoS_{2/3}Se_{4/3}$, whereas in $WS_{2(1-x)}Se_{2x}$ alloys, $WS_{4/3}Se_{2/3}$ is the most stable, and the stability follows $WS_{4/3}Se_{2/3}$ >WSSe > $WS_{2/3}Se_{4/3}$. The magnitude of the ΔH of these ground states is rather small, about −3 meV per anion. In addition, it can be seen from Fig. 1 that the ΔH for random $MoS_{2(1-x)}Se_{2x}$ and $WS_{2(1-x)}Se_{2x}$ alloys are very close to zero, which is consistent with the results of Komsa and Krasheninnikov.[23] Therefore, complete miscibility in these alloys can be achieved at very low temperatures.

The presence of negative ΔH in (S,Se) alloys is somewhat unexpected, as in most semiconductor alloys ΔH is positive. Here, we take the MoSSe as an example for further discussion. The formation of the alloy can be decomposed into three steps:[25] (i) VD: compression or expansion of the equilibrium lattice constant and the bond length of the constituents to the corresponding concentration averaged values; (ii) charge exchange (CEX): construct unrelaxed alloy supercell using the deformed cell in (i) and mix the two types of anions into the lattice; and (iii) SR: fully relax the alloy supercell using quantum mechanical forces. The formation enthalpy ΔH can be then decomposed as: $\Delta H = \Delta H_{VD} + \Delta H_{CEX} + \Delta H_{SR}$. The calculated ΔH_{VD}, ΔH_{CEX}, and ΔH_{SR} for MoSSe are 70.0 meV, −13.9 meV, and −59.5 meV, respectively. The result reveals that the residual strain energy in MoSSe is small, as the positive ΔH_{VD} is largely compensated for by ΔH_{SR}, which can be easily understood by the small lattice mismatch (~4%) between MS_2 and MSe_2. However, $\Delta H_{VD} + \Delta H_{SR}$ is still positive, indicating the SR process alone cannot stabilize the ordered structure. Hence, the negative ΔH_{CEX} is another key role in the formation of ordered alloy. In contrast, many conventional semiconductor alloys has positive ΔH_{CEX}, which leads to destabilization[25] According to a Madelung energy model, the sign of ΔH_{CEX} for a ternary alloy A(B,C) depends on the additional charge exchange $(\Delta Q/\Delta q)$,[25] where $\Delta q = q_B(AB) - q_C(AC)$ is the charge difference between B and C in the two constituents, and $\Delta Q = q_B[A(B,C)] - q_C[A(B,C)]$ is the corresponding difference in the alloy. ΔH_{CEX} becomes negative when $\Delta Q/\Delta q$ is large and exceeds a critical value (typically smaller than 2).[25] The calculated $\Delta Q/\Delta q$ for MoSSe is 1.92, which is likely to result in the negative ΔH_{CEX}. Overall, the formation of the ordered (S,Se) alloys can be attributed to the small lattice mismatch between the constituents and the large additional charge exchange in the alloys.

The formation enthalpies of (Se,Te) and (S,Te) alloys are shown in Fig. 3. The ΔH for all alloy configurations (~17 000) are positive, which differs from the cases of (S,Se) alloy. The positive ΔH can be attributed to the relatively larger lattice mismatch between the two constituent compounds of the alloy. Although the ΔH_{CEX} is also negative for some specific configurations as in the case of (S, Se) alloy, it is overcompensated by the large strain energy. Moreover, the size difference between S and Te is larger than that between Se and Te, thus the ΔH in (S,Te) alloy is larger than that in (Se,Te) alloy. It is also observed that the Mo alloys have lower ΔH than the corresponding W alloys,

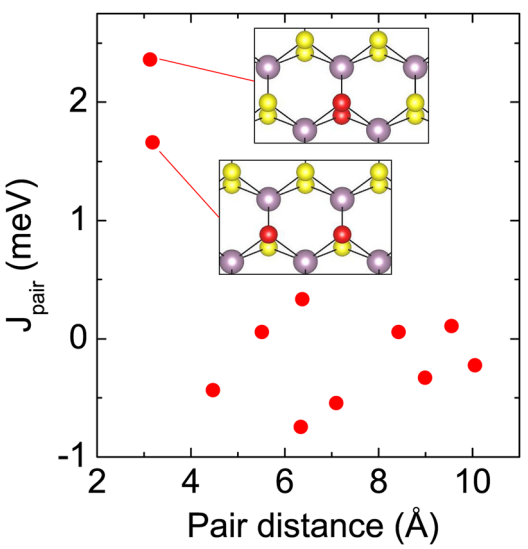

FIG. 2. Effective pair interaction J_{pair} of $MoS_{2(1-x)}Se_{2x}$ as a function of pair distance. Inset: The cluster figures (red balls) associated with the two largest positive J values.

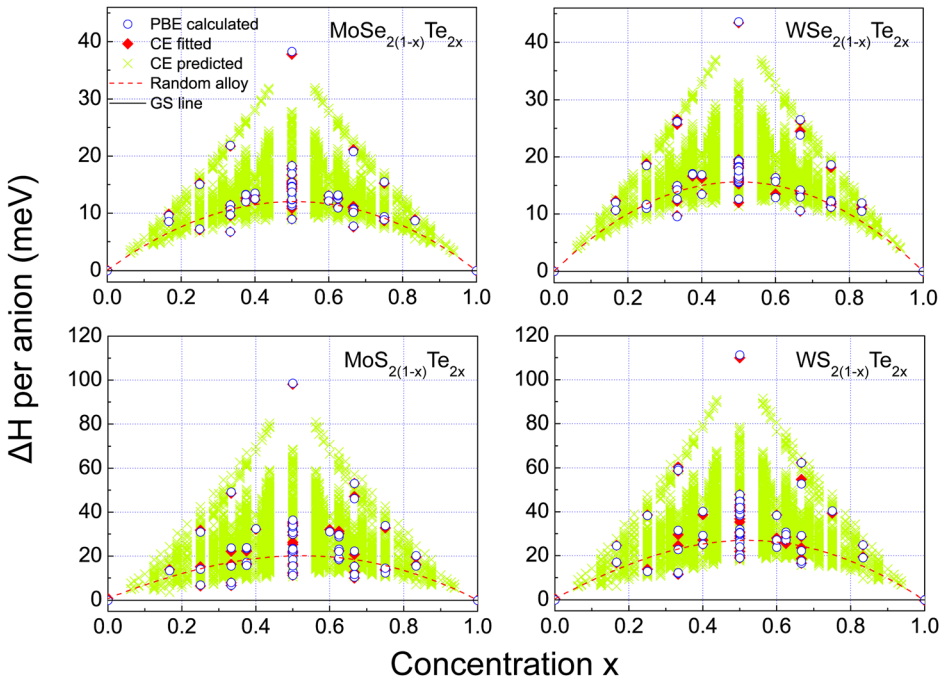

FIG. 3. First-principles calculated, CE fitted and CE predicted formation enthalpies for $MoSe_{2(1-x)}Te_{2x}$, $WSe_{2(1-x)}Te_{2x}$, $MoS_{2(1-x)}Te_{2x}$, and $WS_{2(1-x)}Te_{2x}$.

which is consistent with the smaller in-plane stiffness (thus smaller strain energy) of MoX_2 compared to WX_2.[5]

The positive ΔH indicates that there is no stable configuration for (Se,Te) and (S,Te) alloys at 0 K, and phase separation will occur. However, the solubility in these alloys can be improved by increasing the temperature. In addition, as seen from Fig. 3, the magnitude of ΔH for these alloys in random configuration is very small, on the order of 10 meV per anion, hence a complete miscibility is possible at experimentally achievable temperatures. Using the constructed CE, the critical temperature for complete miscibility (T_{CM}) of (Se,Te) and (S,Te) alloys can be estimated analytically. The free energy $F(x,T)$ of a random alloy at temperature T with concentration x is defined as

$$F(x,T) = \Delta H(x) - TS(x),$$

where $\Delta H(x)$ is the formation enthalpy, which can be calculated by the fitted CE and correlation functions of the random alloy. $S(x)$ is the entropy, and can be estimated within a mean-field approximation,[35,36]

$$S(x) = -k_B[x\ln x + (1-x)\ln(1-x)]$$

with k_B being the Boltzman constant. The binodal line on the phase diagram can then be derived by applying the common tangent construction to the F-x curves at different temperatures.[37] The calculated phase diagrams are shown in Fig. 4. The binodal lines of (Se,Te) alloys are nearly symmetric, which can be attributed to their negligible point and triplet ECIs. However, an asymmetric solubility is predicted for (S,Te) alloys. Therefore, at a given temperature, mixing Te atoms into MS_2 is easier than mixing S atoms into MTe_2, and this asymmetry is enhanced with increasing temperature. This occurs because the point and triplet ECIs cannot be neglected in (S,Te) alloys. The point ECIs in (S,Te) alloys are found to be positive, which make the dissolution of Te easier. The estimated T_{CM} for $MoSe_{2(1-x)}Te_{2x}$, $WSe_{2(1-x)}Te_{2x}$, $MoS_{2(1-x)}Te_{2x}$, and $WS_{2(1-x)}Te_{2x}$ is about 279 K, 360 K, 493 K, and 687 K, respectively. The values of T_{CM} follow the trend of formation enthalpies: T_{CM} of (S,Te) alloys is higher than that of (Se,Te) alloys, and T_{CM} of W alloys is higher than that of Mo alloys. $WS_{2(1-x)}Te_{2x}$ has the highest T_{CM} of ~687 K, which is experimentally easily accessible. It should also be noted that lattice vibration is neglected in the mean-field approximation for entropy; therefore, the solubility is underestimated, and the actual T_{CM}

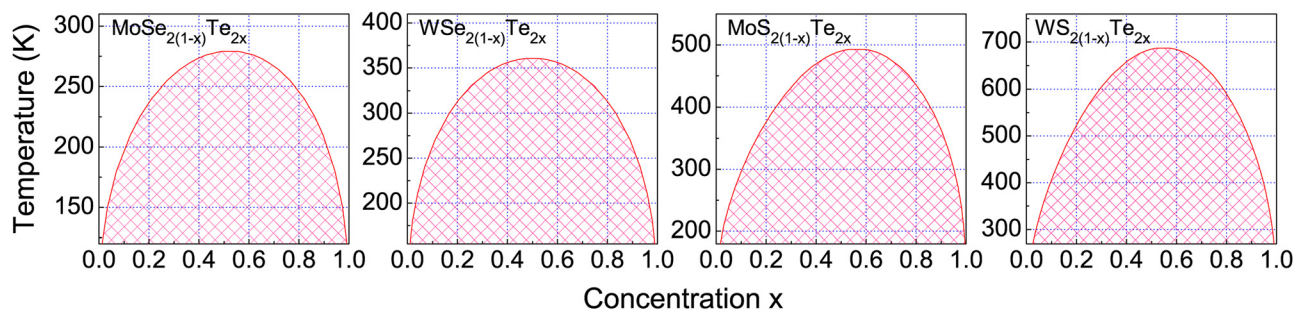

FIG. 4. Phase diagrams for $MoSe_{2(1-x)}Te_{2x}$, $WSe_{2(1-x)}Te_{2x}$, $MoS_{2(1-x)}Te_{2x}$, and $WS_{2(1-x)}Te_{2x}$. The areas of phase separation are shaded.

would be even lower than the estimated values. Therefore, a class of complete miscible $MX_{2(1-x)}X'_{2x}$ alloys is experimentally achievable in principle.

B. Bowing effects

In most cases, a quadratic rule can be used to describe the relationship between physical properties P and concentration x of the alloy $A_{(1-x)}B_x$, namely,

$$P(x) = (1-x)P(A) + xP(B) - bx(1-x),$$

where b is the bowing parameter. Usually, the bowing parameter of lattice constant is negligible, leading to a linear relationship, which is known as the Vegard's law. On the other hand, the bowing of band gap and band edge position is often significant. In this section, we investigate the bowing parameters of $MX_{2(1-x)}X'_{2x}$ random alloys for lattice constant, band gap, VBM, and CBM positions, using the 6×6 SQS as described above.

After full relaxation, the honeycomb structure in $MX_{2(1-x)}X'_{2x}$ alloys is preserved, and the lattice constant as a function of x is shown in Fig. 5. The calculated bowing parameters are small, as seen in Table I, hence the lattice constants scale almost linearly with x, indicating that these alloys obey the Vegard's law. The maximum bowing parameter is 0.08 Å, corresponding to a deviation of only 0.02 Å from the linear relationship at $x = 0.5$. Despite the considerable different lattice constant between MX_2 and MX'_2, it is observed that the M-X and M-X′ bond lengths in the $MX_{2(1-x)}X'_{2x}$ alloys are almost the same as in the pure MX_2 and MX'_2. This bond length conservation can be understood by (i) the anions are not confined along the perpendicular direction due to the 2D feature, and (ii) the M-X bond has a strong ionic character, so that the directionality is relatively weak. These two factors lead to an extremely small ratio of bond-bending force over bond-stretching force. Hence, the M-X bonds can be bent much more easily than be stretched, resulting in the bond length conservation in the alloys.

The band gaps of $MX_{2(1-x)}X'_{2x}$ random alloys are plotted in Fig. 5. In pure MX_2 monolayer, the band gap is direct, with the CBM and VBM located at the K point. The calculated band gaps for $MX_{2(1-x)}X'_{2x}$ alloys are also direct, and the CBM and VBM are located at the Γ point instead. The change in the position of band edges results from zone-folding effect. For the alloy calculation, a 6×6 supercell was used here, and the K point in the Brillouin zone of a primitive hexagonal cell will be folded into the Γ point in the Brillouin zone of the 6×6 supercell. By projecting the band edge states into the atomic orbitals, it is found that the CBM and VBM of the alloys have the same orbital characters as those of pure MX_2, i.e., the CBM state consists mainly of the d_{z^2} orbital of cations and the p_x and p_y orbitals of anions, while the VBM state consists of the $d_{x^2-y^2}$ and d_{xy} orbitals of cations and the p_x and p_y orbitals of anions.

Therefore, the band gap value of MX_2 monolayers can be tuned over a wide range of 1.0 – 1.8 eV by alloying, whereas the direct gap character is maintained, which is favorable for optoelectronic applications. In contrast, although the band gap of MX_2 can be also tuned by strain,[10,11] the range of strain that retains the direct gap is quite limited. We also note that the 1.0 – 1.8 eV range is a very relevant spectral range for photovoltaic applications,[38] where fine tuning of band gap is desired for maximal energy conversion efficiency. The bowing parameters of band gaps (b_{Gap}) for the alloys are listed in Table I. All b_{Gap} are positive, and their magnitude is typically less than 0.5 eV. As the size and chemical differences between the two constituent compounds increase, the gap bowing effect in the alloy becomes more significant. For example, $MoS_{2(1-x)}Se_{2x}$ has a quite small b_{Gap} of 0.05 eV, whereas b_{Gap} of $MoS_{2(1-x)}Te_{2x}$ increases to 0.41 eV.

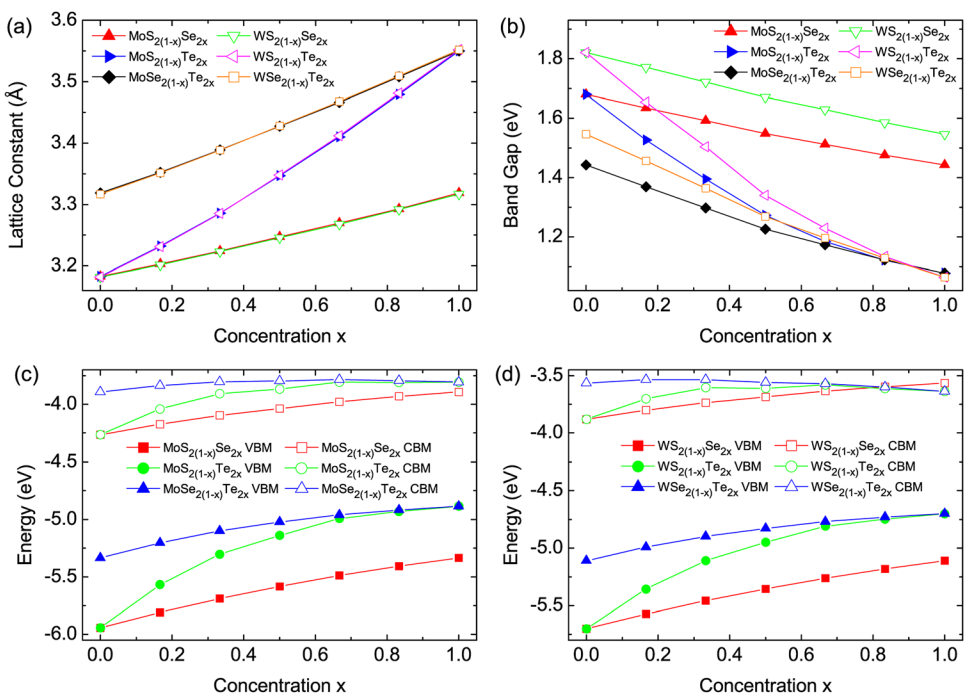

FIG. 5. (a) Lattice constant of $MX_{2(1-x)}X'_{2x}$ alloys as a function of concentration x. (b) The band gap of $MX_{2(1-x)}X'_{2x}$ alloys as a function of concentration. (c) and (d) The VBM and CBM positions of Mo and W alloys as a function of concentration. The vacuum level is taken as zero energy reference.

TABLE I. Bowing parameters for the lattice constant (b_{lat}), band gap (b_{Gap}), VBM position (b_{VB}), and CBM position (b_{VB}) of $MX_{2(1-x)}X'_{2x}$ random alloys, as well as the decomposed bowing parameters for band gap and band edge positions in the VD, CEX, and SR processes.

		Total			VD			CEX			SR		
	b_{lat} (Å)	b_{Gap} (eV)	b_{VB} (eV)	b_{CB} (eV)	b_{Gap} (eV)	b_{VB} (eV)	b_{CB} (eV)	b_{Gap} (eV)	b_{VB} (eV)	b_{CB} (eV)	b_{Gap} (eV)	b_{VB} (eV)	b_{CB} (eV)
$MoS_{2(1-x)}Se_{2x}$	0.02	0.05	−0.22	−0.18	0.02	0.08	0.10	0.05	−0.10	−0.05	−0.03	−0.20	−0.23
$MoSe_{2(1-x)}Te_{2x}$	0.03	0.12	−0.36	−0.24	0.07	0.20	0.27	0.12	−0.20	−0.08	−0.07	−0.36	−0.43
$MoS_{2(1-x)}Te_{2x}$	0.08	0.41	−1.17	−0.76	0.19	0.52	0.70	0.33	−0.61	−0.28	−0.11	−1.08	−1.19
$WS_{2(1-x)}Se_{2x}$	0.02	0.04	−0.21	−0.16	0.02	0.09	0.11	0.04	−0.10	−0.06	−0.02	−0.20	−0.22
$WSe_{2(1-x)}Te_{2x}$	0.03	0.12	−0.32	−0.20	0.10	0.23	0.33	0.09	−0.20	−0.11	−0.06	−0.35	−0.41
$WS_{2(1-x)}Te_{2x}$	0.08	0.36	−1.06	−0.70	0.24	0.55	0.79	0.24	−0.56	−0.32	−0.12	−1.05	−1.17

The CBM and VBM positions of the alloys are also calculated and shown in Fig. 5, as well as listed in Table I. The trends of b_{VB} and b_{CB} are similar to b_{Gap}, i.e., larger size and chemical differences lead to larger bowing. It is interesting to note that both b_{VB} and b_{CB} are negative, namely, both VBM and CBM show upward bowing, and the bowing in the band edge positions is much more significant than in the band gap. The weak bowing in band gap is a consequence of partial mutual cancellation of the strong CBM and VBM bowing. In contrast, in most traditional semiconductor alloys such as ZnSTe,[39] GaNAs,[40] and SnGe,[41] VBM shows upward bowing while CBM shows downward bowing. This stark difference possibly originates from the unique character of band edge states in $MX_{2(1-x)}X'_{2x}$ distinctly different from traditional semiconductors. The band bowing in semiconductor alloys is typically caused by different deformation potentials of the constituents, as well as coupling of states through the potential difference ΔV between the alloy potential and the average potential of the constituents.[18,42] ΔV induces intra-band coupling within the conduction band (CB) and valence band (VB), and inter-band coupling between them. The inter-band coupling raises the CBM and lowers the VBM, whereas the intra-band coupling lowers the CBM and raises the VBM.[18] In traditional semiconductors, VBM is mostly p-like and CBM is mostly s-like. Because of the very different orbital characters between VBM and CBM, the intra-band coupling is much stronger than the inter-band coupling, leading to the upward (downward) bowing of VBM (CBM). However, in $MX_{2(1-x)}X'_{2x}$ alloys both VBM and CBM are d-like, and the inter-band coupling is much enhanced, leading to the upward bowing of CBM.

Similar to other semiconductor alloys, the bowing of band gap and band edge position in $MX_{2(1-x)}X'_{2x}$ can also be decomposed to the above mentioned three parts VD, CEX, and SR.[43] The bowing parameter for each process is calculated, and listed in Table I, and the total bowing parameter is given by $b = b_{VD} + b_{CEX} + b_{SR}$. The following results are observed:

(i) The sign of the VBM bowing parameters is the same as the CBM bowing in all three processes. The VD induced VBM and CBM bowing is positive; the positive b_{VD} is partially compensated by the CEX and SR processes, where b_{VB} and b_{CB} are negative, and the total b_{VB} and b_{CB} become negative. The band gap bowing in each process is much smaller, resulting from the partial cancellation of VBM and CBM bowing.

(ii) In the VD and SR processes, the CBM bowing is more obvious than the VBM bowing. These two processes displace relative positions of anions and cations, and the CBM state is more sensitive to such displacements, so its bowing is more distinct. This contributes to positive and negative gap bowing in VD and SR, respectively. In the CEX process, the VBM bowing is more significant, and this contributes to a positive band gap bowing. This occurs because: first of all, the VBM state of the MX_2 has more anion p character than the CBM state, resulting in larger influence on VBM than on CBM when different anions are mixed. Second, we find that the original valence band offset between different MX_2 is larger than the conduction band offset;[44] therefore, the chemical difference between VBM is larger than between CBM.

(iii) The values of the bowing parameters for the VD, CEX, and SR processes are on the same order, indicating that both lattice mismatch and chemical potential difference are important factors responsible for the band gap and band edge position bowing in $MX_{2(1-x)}X'_{2x}$ alloys. The contribution of SR to the VBM and CBM bowing is the largest, indicating a unusually large structure relaxation in $MX_{2(1-x)}X'_{2x}$ alloys, which is enhanced by their 2D nature as discussed above.

(iv) All bowing parameters follow the trend $|b(S,Te)| > |b(Se,Te)| > |b(S,Se)|$. Such an order is not surprising given that the size mismatch and chemical potential difference increase from S-Se, Se-Te, to S-Te.

IV. CONCLUSIONS

We have constructed cluster expansion for $MX_{2(1-x)}X'_{2x}$ alloys, and studied their stability and miscibility based on the fitted effective cluster interactions. The bowing effects in these alloys are discussed. Our findings can be summarized as:

(i) In (S,Se) alloys, there exist stable ordered alloy structures even at 0 K with concentration x of of 1/3, 1/2, and 2/3. Clustering of S or Se atoms is not favored

because of the dominance of positive cluster interactions of short-range pairs. The ordered structure results from the small lattice mismatch between the constituents and the large additional charge exchange in the alloys. The formation enthalpies of random alloys are close to zero, so a complete miscibility can be achieved at very low temperatures.

(ii) In (Se,Te) and (S,Te) alloys, there is no stable alloy configuration at 0 K, and phase separation into the two constituents will occur. Nevertheless, the miscibility in these alloys can be much enhanced by increasing temperature, and the calculated phase diagrams show that a complete miscibility can be achieved at moderate temperatures. In addition, an asymmetric solubility line is observed in (S,Te) alloys, which can be attributed to non-negligible contributions of point and triplet cluster interactions.

(iii) The lattice constant of $MX_{2(1-x)}X'_{2x}$ alloys scale almost linearly with x; compared with the pure binary compounds, the cation-anion bond lengths remain the same in the alloys. The bond length conservation is a result of the 2D nature and ionic bond character in the alloys.

(iv) The band gap and band edge position of $MX_{2(1-x)}X'_{2x}$ varies as a function of the concentration x. More importantly, the direct gap character of MX_2 monolayer is retained in the alloys. The band gap shows a downward (positive) bowing, while the CBM and VBM show an unusual upward bowing; the bowing of the band edge position is much more significant than that of band gap. By decomposing the formation of alloy into three steps, it is found that the bowing effect in the alloys is a joint effect of volume deformation, chemical difference, and a low-dimensionality enhanced structure relaxation; larger size mismatch and chemical potential difference result in to higher bowing parameter.

ACKNOWLEDGMENTS

J. Li gratefully acknowledges financial support from the National Science Fund for Distinguished Young Scholar (Grant No. 60925016). This work was supported by the National Basic Research Program of China (Grant No. 2011CB921901) and the External Cooperation Program of Chinese Academy of Sciences. We acknowledge the computing resources provided by the Supercomputing Center, CNIC, CAS.

[1]K. S. Novoselov, D. Jiang, F. Schedin, T. J. Booth, V. V. Khotkevich, S. V. Morozov, and A. K. Geim, Proc. Natl. Acad. Sci. U.S.A. **102**, 10451 (2005).
[2]J. N. Coleman, M. Lotya, A. ONeill, S. D. Bergin, P. J. King, U. Khan, K. Young, A. Gaucher, S. De, R. J. Smith, I. V. Shvets, S. K. Arora, G. Stanton, H.-Y. Kim, K. Lee, G. T. Kim, G. S. Duesberg, T. Hallam, J. J. Boland, J. J. Wang, J. F. Donegan, J. C. Grunlan, G. Moriarty, A. Shmeliov, R. J. Nicholls, J. M. Perkins, E. M. Grieveson, K. Theuwissen, D. W. McComb, P. D. Nellist, and V. Nicolosi, Science **331**, 568 (2011).
[3]Z. Zeng, Z. Yin, X. Huang, H. Li, Q. He, G. Lu, F. Boey, and H. Zhang, Angew. Chem., Int. Ed. **50**, 11093 (2011).
[4]S. Tongay, J. Zhou, C. Ataca, K. Lo, T. S. Matthews, J. Li, J. C. Grossman, and J. Wu, Nano Lett. **12**, 5576 (2012).
[5]C. Ataca, H. Şahin, and S. Ciraci, J. Phys. Chem. C **116**, 8983 (2012).
[6]K. S. Novoselov, A. K. Geim, S. V. Morozov, D. Jiang, Y. Zhang, S. V. Dubonos, I. V. Grigorieva, and A. A. Firsov, Science **306**, 666 (2004).
[7]Y. Ding, Y. Wang, J. Ni, L. Shi, S. Shi, and W. Tang, Physica B **406**, 2254 (2011).
[8]K. F. Mak, C. Lee, J. Hone, J. Shan, and T. F. Heinz, Phys. Rev. Lett. **105**, 136805 (2010).
[9]A. Splendiani, L. Sun, Y. Zhang, T. Li, J. Kim, C.-Y. Chim, G. Galli, and F. Wang, Nano Lett. **10**, 1271 (2010).
[10]W. S. Yun, S. W. Han, S. C. Hong, I. G. Kim, and J. D. Lee, Phys. Rev. B **85**, 033305 (2012).
[11]P. Johari and V. B. Shenoy, ACS Nano **6**, 5449 (2012).
[12]A. Ramasubramaniam, Phys. Rev. B **86**, 115409 (2012).
[13]T. Cao, G. Wang, W. Han, H. Ye, C. Zhu, J. Shi, Q. Niu, P. Tan, E. Wang, B. Liu, and J. Feng, Nat. Commun. **3**, 887 (2012).
[14]H. Zeng, J. Dai, W. Yao, D. Xiao, and X. Cui, Nat. Nanotechnol. **7**, 490 (2012).
[15]Z. Yin, H. Li, H. Li, L. Jiang, Y. Shi, Y. Sun, G. Lu, Q. Zhang, X. Chen, and H. Zhang, ACS Nano **6**, 74 (2012).
[16]B. Radisavljevic, A. Radenovic, J. Brivio, V. Giacometti, and A. Kis, Nat. Nanotechnol. **6**, 147 (2011).
[17]B. Radisavljevic, M. B. Whitwick, and A. Kis, ACS Nano **5**, 9934 (2011).
[18]S.-H. Wei and A. Zunger, J. Appl. Phys. **78**, 3846 (1995).
[19]S.-H. Wei, S. B. Zhang, and A. Zunger, J. Appl. Phys. **87**, 1304 (2000).
[20]D. Korakakis, J. K. F. Ludwig, and T. D. Moustakas, Appl. Phys. Lett. **71**, 72 (1997).
[21]G. P. Srivastava, J. L. Martins, and A. Zunger, Phys. Rev. B **31**, 2561 (1985).
[22]J. E. Bernard, R. G. Dandrea, L. G. Ferreira, S. Froyen, S.-H. Wei, and A. Zunger, Appl. Phys. Lett. **56**, 731 (1990).
[23]H.-P. Komsa and A. V. Krasheninnikov, J. Phys. Chem. Lett. **3**, 3652 (2012).
[24]J. Sanchez, F. Ducastelle, and D. Gratias, Physica A **128**, 334 (1984).
[25]L. G. Ferreira, S.-H. Wei, and A. Zunger, Phys. Rev. B **40**, 3197 (1989).
[26]A. Zunger, S.-H. Wei, L. G. Ferreira, and J. E. Bernard, Phys. Rev. Lett. **65**, 353 (1990).
[27]A. van de Walle, M. Asta, and G. Ceder, CALPHAD: Comput. Coupling Phase Diagrams Thermochem. **26**, 539 (2002).
[28]S.-H. Wei, L. G. Ferreira, J. E. Bernard, and A. Zunger, Phys. Rev. B **42**, 9622 (1990).
[29]G. Kresse and J. Hafner, Phys. Rev. B **47**, 558 (1993).
[30]G. Kresse and J. Furthmüller, Phys. Rev. B **54**, 11169 (1996).
[31]P. E. Blöchl, Phys. Rev. B **50**, 17953 (1994).
[32]G. Kresse and D. Joubert, Phys. Rev. B **59**, 1758 (1999).
[33]J. P. Perdew, K. Burke, and M. Ernzerhof, Phys. Rev. Lett. **77**, 3865 (1996).
[34]H. J. Monkhorst and J. D. Pack, Phys. Rev. B **13**, 5188 (1976).
[35]W. R. L. Lambrecht and B. Segall, Phys. Rev. B **47**, 9289 (1993).
[36]B. Alling, A. V. Ruban, A. Karimi, O. E. Peil, S. I. Simak, L. Hultman, and I. A. Abrikosov, Phys. Rev. B **75**, 045123 (2007).
[37]L. K. Teles, J. Furthmüller, L. M. R. Scolfaro, J. R. Leite, and F. Bechstedt, Phys. Rev. B **62**, 2475 (2000).
[38]Q. H. Wang, K. Kalantar-Zadeh, A. Kis, J. N. Coleman, and M. S. Strano, Nat. Nanotechnol. **7**, 699 (2012).
[39]J. Wu, W. Walukiewicz, K. M. Yu, J. W. Ager, E. E. Haller, I. Miotkowski, A. K. Ramdas, C.-H. Su, I. K. Sou, R. C. C. Perera, and J. D. Denlinger, Phys. Rev. B **67**, 035207 (2003).
[40]J. Wu, W. Walukiewicz, K. M. Yu, J. D. Denlinger, W. Shan, J. W. Ager, A. Kimura, H. F. Tang, and T. F. Kuech, Phys. Rev. B **70**, 115214 (2004).
[41]W.-J. Yin, X.-G. Gong, and S.-H. Wei, Phys. Rev. B **78**, 161203 (2008).
[42]S.-H. Wei and A. Zunger, Phys. Rev. B **43**, 1662 (1991).
[43]J. E. Bernard and A. Zunger, Phys. Rev. B **34**, 5992 (1986).
[44]J. Kang, S. Tongay, J. Zhou, J. Li, and J. Wu, Appl. Phys. Lett. **102**, 012111 (2013).